chemistry

MDPI

Article

Improved Synthesis and Coordination Behavior of 1*H*-1,2,3-Triazole-4,5-dithiolates ($tazdt^{2-}$) with Ni^{II}, Pd^{II}, Pt^{II} and Co^{III}

Nils Pardemann [1], Alexander Villinger [1] and Wolfram W. Seidel [1,2,*]

[1] Institut für Chemie, Universität Rostock, Albert-Einstein-Straße 3a, 18059 Rostock, Germany
[2] Leibniz-Institut für Katalyse e.V., Albert-Einstein-Straße 29a, 18059 Rostock, Germany
* Correspondence: wolfram.seidel@uni-rostock.de

Abstract: A new synthetic route to 1*H*-1,2,3-triazole-4,5-dithiols ($tazdtH_2$) as ligands for the coordination of Ni^{II}, Pd^{II}, Pt^{II} and Co^{III} via the dithiolate unit is presented. Different N-protective groups were introduced with the corresponding azide via a click-like copper-catalyzed azide-alkyne [3 + 2] cycloaddition (CuAAC) and fully characterized by NMR spectroscopy. Possible isomers were isolated and an alternative synthetic route was investigated and discussed. After removal of the benzyl protective groups on sulfur by in situ-generated sodium naphthalide, complexes at the [(dppe)M] (M = Ni, Pd, Pt), $[(PPh_3)_2Pt]$ and $[(\eta^5\text{-}C_5H_5)Co]$ moieties were prepared and structurally characterized by XRD analysis. In this process, the by-products **11** and **12** as monothiolate derivatives were isolated and structurally characterized as well. With regioselective coordination via the dithiolate unit, the electronic influence of different metals or protective groups at N was investigated and compared spectroscopically by means of UV/Vis spectroscopy and cyclic voltammetry. Complex $[(\eta^5\text{-}C_5H_5)Co(\mathbf{5c})]$ (**10**), is subject to a dimerization equilibrium, which was investigated by temperature-dependent NMR and UV/Vis spectroscopy (solution and solid-state). The thermodynamic parameters of the monomer/dimer equilibrium were derived.

Keywords: dithiolene complex; 1,2,3-triazole ligands; click chemistry; CuAAC; thiol protective groups

check for updates

Citation: Pardemann, N.; Villinger, A.; Seidel, W.W. Improved Synthesis and Coordination Behavior of 1*H*-1,2,3-Triazole-4,5-dithiolates ($tazdt^{2-}$) with Ni^{II}, Pd^{II}, Pt^{II} and Co^{III}. *Chemistry* **2023**, *5*, 1271–1287. https://doi.org/10.3390/chemistry5020086

Academic Editors: Christoph Janiak, Sascha Rohn and Georg Manolikakes

Received: 11 April 2023
Revised: 9 May 2023
Accepted: 10 May 2023
Published: 17 May 2023

1. Introduction

The award of the Nobel Prize to Sharpless, Meldal and Bertozzi in 2022 represents an accolade for click chemistry as a powerful synthetic method [1]. The concept of click chemistry was established as early as 2001 and describes a rapid and precise synthesis of molecules following the example of nature. The advantages of the method are high atomic efficiency, very few by-products and high yields while only the use of cheap and simple chemicals and short reaction time are needed [2]. Classically, click chemistry often includes Diels–Alder reactions, addition reactions on carbon–carbon double bonds, and especially copper-catalyzed Huisgen cycloaddition, which can be used for the synthesis of 1*H*-1,2,3-triazoles [3–5]. Sharpless and coworkers presented first protocols for the [3 + 2] cycloaddition of azides with terminal alkynes under Cu-catalyzed reaction conditions [5]. A [3 + 2] cycloaddition between azides and acetylenes are not regioselective [6–8]. Two regioisomeres with a substituent in 4- or 5-position are formed. Only in the case of electrophilically activated acetylenes is high regioselectivity possible [5,9,10]. The copper-catalyzed azide-alkyne [3 + 2] cycloaddition (CuAAC) opens a way for the regioselective synthesis of triazoles. In addition to various alkyl and aryl substituents, donors such as phosphanes, amines, sulfur and seleniums could be introduced into the 1*H*-1,2,3-triazole system as well [11–16]. Introduction of thiol groups at both 4- and 5-position of the triazole would result in a new ligand with five potential coordination sites in the form of the dithiolene unit and the N atoms. Both through the aromatic properties of the 1*H*-1,2,3-triazole ring and through the specific electronic situation of the dithiolene unit, the 1*H*-1,2,3-triazole-4,5-dithiolate ($tazdt^{2-}$) could serve as a versatile

bridging ligand between several metal centers. In particular, the electronic properties appear potentially interesting due to the non-innocent character of the dithiolene unit [17–19]. In contrast to many other triazoles, a synthesis of 1*H*-1,2,3-triazole-4,5-dithiols by means of a click-like copper-catalyzed azide-alkyne [3 + 2] cycloaddition is not known to the best of our knowledge. So far, synthesis of 1*H*-1,2,3-triazole-4,5-disulfides was reported in a Ru-catalyzed [3 + 2] cycloaddition of an azide and a bis(alkylsulfanyl) acetylene at high temperatures under inert gas atmosphere [16,20]. Alternatively, this synthesis can be carried out with [(NHC)CuI] (NHC = 1-benzyl-3-*n*-butyl-1*H*-benz[*d*] imidazolylidene) as catalyst. The latter is easier to use, but the yields are lower compared with the Ru-based catalyst. In addition, 1*H*-1,2,3-triazoles have been synthesized in an Ir-catalyzed [3 + 2] cycloaddition of internal mono(alkylsulfanyl)alkynes with an azide [21]. Herein, we present a substantially improved synthesis of 1*H*-1,2,3-triazole-4,5-disulfides under CuAAC click conditions using the terminal benzylsulfanylacetylene. Pitfalls of the reductive removal of S-protective benzyl groups are identified by isolation of respective thiolato complexes. Finally, we describe coordination of the corresponding dithiols to group 10 metals and Co^{III}. The influence of the metal and the N-protective groups at the triazole on the electronic properties will be discussed.

2. Materials and Methods

2.1. Chemical Reagents and Instruments

Materials, details on physical measurements, X-ray determination data, original NMR and IR spectra of all products and preparative procedures as well as spectroscopic data of the only organic products (**1**–**4**) are provided in the ESI.

2.2. Synthetic Protocols

2.2.1. General Synthesis of **5**

A solution of **2a**–**c** (1 mmol) in THF (50 mL) was treated with sodium (5 mmol) and naphthalene (2.5 mmol). The red-brown suspension was stirred overnight, then cooled to 0 °C. MeOH (10 mL) was added and the mixture was stirred until gas evolution ceased. For purification, the solution was dried in vacuo, taken up in H_2O (40 mL) and washed three times with Et_2O (10 mL aliquots). The aqueous fraction was filtered over celite in a G3 frit and subsequently acidified with aqueous HCl (pH = 3–4), leading to the formation of a beige precipitate. The suspension was extracted four times with CH_2Cl_2 (aliquots of 10 mL). The organic fraction was dried over Na_2SO_4, filtered and dried in vacuo to isolate **5** as crude products. According to NMR, the samples are not analytically but sufficiently pure for successful complex synthesis. Potential by-products were characterized in the form of stable complexes as well (see compounds **11** and **12**).

H_2-**5a**, 1.049 g (2.42 mmol) **2a**, 0.284 g (12.35 mmol) sodium, 0.777 g (6.06 mmol) naphthalene: yield 0.174 g (28%, crude product). ^{1}H NMR ($CDCl_3$, δ, ppm, 300 MHz, 298 K): 7.25–7.22 (m, 2 H, *H*-*o*-(4-MOB)), 6.92–6.89 (m, 2 H, *H*-*m*-(4-MOB)), 5.45 (s, 2 H, NCH_2), 3.81 (s, 3 H, CH_3) + additional by-product signals. IR (CH_2Cl_2, $\tilde{\nu}$, cm^{-1}): 3686 (m), 2978 (s), 2873 (s), 2362 (w), 1604 (m), 1510 (m), 1384 (m), 1274 (s), 1110 (s), 763 (s), 697 (s).

H_2-**5b**, 0.649 g (1.401 mmol) **2b**, 0.165 g (7.174 mmol) sodium, 0.834 g (6.507 mmol) naphthalene: yield 0.323 g (40%, crude product). ^{1}H NMR (CD_2Cl_2, δ, ppm, 300 MHz, 298 K): 7.20–7.17 (m, 1 H, *H*-(2,4-dMOB)), 6.51–6.48 (m, 2 H, *H*-(2,4-dMOB)), 5.56 (s, 2 H, NCH_2), 3.82 (s, 3 H, CH_3), 3.79 (s, 3 H, CH_3) + additional by-product signals. IR (CH_2Cl_2, $\tilde{\nu}$, cm^{-1}): 2994 (s), 2890 (s), 2824 (s), 2496 (w), 1618 (s), 1509 (s), 1465 (m), 1300 (s), 1210 (s), 1157 (s), 1067 (s), 1038 (s), 901 (s), 840 (m), 697 (m).

H_2-**5c**, 0.632 g (1.53 mmol) **2c**, 0.173 g (7.52 mmol) sodium, 0.496 g (3.87 mmol) naphthalene: yield 0.356 g (76%, crude product). ^{1}H NMR (THF-D_8, δ, ppm, 300 MHz, 298 K): 4.57–4.31 (m, 2 H, NCH_2), 1.32–1.18 (m, 2 H, CH_2TMS), 0.07 (s, 9 H, CH_3-TMS) + additional by-product signals.

2.2.2. General Synthesis of the Metal Complexes **6** and **7**

In a 50 mL flask 1 equivalent [(dppe)MCl_2] (M = Ni, Pd) was suspended in 15 mL H_2O. A solution of 1.1 equivalents **5b** in CH_2Cl_2 (25 mL) and 3 equivalents KOH were subsequently added. In the two-phase system, a color change from red to green (Ni) or colorless to violet (Pd) was observed in the lower phase. The reaction system was stirred for 3 days at room temperature. To purify the product, the aqueous phase was removed and the organic fraction washed four times with H_2O (15 mL), dried over Na_2SO_4 and filtered and the solvent was removed in vacuo. A column chromatographic purification was carried out with a CH_2Cl_2/MeOH solvent mixture (20/1) as a mobile phase. Suitable crystals for X-ray structure analysis were obtained from a CH_2Cl_2 solution by slow diffusion of *n*-pentane.

[(dppe)Ni(**5b**)] (**6**), 0.115 g (0.22 mmol) [(dppe)$NiCl_2$], 0.077 g (1.37 mmol) KOH, 0.068 g (approx. 0.24 mmol) **5b**: yield, 0.086 g (54%). Anal. Calcd. for $C_{37}H_{35}N_3NiO_2P_2S_2$: C, 60.18; H, 4.78; N, 5.69; S, 8.68%. Found: C, 59.79; H, 4.71; N, 5.77; S, 8.57%. ^{1}H NMR ($CDCl_3$, δ, ppm, 300 MHz, 298 K): 7.83–7.75 (m, 8 H, *H*-Ph), 7.52–7.43 (m, 12 H, *H*-Ph), 6.93 (d, $^3J_{H,H}$ = 8.3 Hz, 1 H, *H-o*-(2,4-dMOB)), 6.32 (d, $J_{H,H}$ = 2.4 Hz, 1 H, *H-m'*-(2,4-dMOB)), 6.28 (dd, $^3J_{H,H}$ = 8.3 Hz, $J_{H,H}$ = 2.4 Hz, 1 H, *H-m*-(2,4-dMOB)), 5.20 (s, 2 H, NCH_2), 3.73 (s, CH_3), 3.61 (s, CH_3), 2.40–2.22 (m, 4 H, CH_2-dppe). ^{13}C NMR ($CDCl_3$, δ, ppm, 75 MHz, 298 K): 160.3 (s, *C*-(2,4-dMOB)), 158.0 (s, *C*-(2,4-dMOB)), 156.7 (s, *C*-tazdt), 145.5 (d, $^3J_{C,P}$ = 17.3 Hz, *C*-tazdt), 133.6 (dd, $^3J_{C,P}$ = 10.6 Hz, $J_{C,P}$ = 2.2 Hz, *C*-Ph), 131.6 (s, *C*-Ph), 130.3 (s, *C*-(2,4-dMOB)), 129.1 (dd, $^1J_{C,P}$ = 46.9 Hz, $^3J_{C,P}$ = 16.1 Hz, *C*-Ph), 129.0 (dd, $^2J_{C,P}$ = 10.7 Hz, $J_{C,P}$ = 2.8 Hz, *C*-Ph), 117.5 (s, *C*-(2,4-dMOB)), 104.2 (s, *C*-(2,4-dMOB)), 98.3 (s, *C*-(2,4-dMOB)), 55.4 (s, CH_3), 55.4 (s, CH_3), 45.5 (s, NCH_2), 27.5–26.8 (m, CH_2-dppe). ^{31}P NMR ($CDCl_3$, δ, ppm, 122 MHz, 298 K): 60.5 (d, $^2J_{P,P}$ = 47.9 Hz, *P*-dppe), 58.7 (d, $^2J_{P,P}$ = 47.9 Hz, *P*-dppe). IR (CH_2Cl_2, $\tilde{\nu}$, cm^{-1}): 2963 (w), 1614 (m), 1508 (m), 1437 (m), 1261 (s), 1208 (m), 1103 (m), 739 (s), 691 (m), 532 (m).

[(dppe)Pd(**5b**)] (**7**), 0.161 g (0.28 mmol) [(dppe)$PdCl_2$], 0.055 g (0.98 mmol) KOH, 0.084 g (approx. 0.30 mmol) **5b**: yield 0.097 g (44%). ^{1}H NMR (DMF-D_7, δ, ppm, 300 MHz, 298 K): 8.03–7.87 (m, 8 H, *H*-Ph), 7.66–7.61 (m, 12 H, *H*-Ph), 6.88 (d, $^3J_{H,H}$ = 8.4 Hz, 1 H, *H-o*-(2,4-dMOB)), 6.60 (d, $J_{H,H}$ = 2.3 Hz, 1 H, *H-m'*-(2,4-dMOB)), 6.49 (dd, $^3J_{H,H}$ = 8.4 Hz, $J_{H,H}$ = 2.3 Hz, 1 H, *H-m*-(2,4-dMOB)), 5.17 (s, 2 H, NCH_2), 3.83 (s, 6 H, CH_3), 3.03–2.86 (m, 4 H, CH_2-dppe). ^{13}C NMR (DMF-D_7, δ, ppm, 75 MHz, 298 K): 160.9 (s, *C*-(2,4-dMOB)), 158.0 (s, *C*-(2,4-dMOB)), 154.5 (dd, $^3J_{C,P}$ = 10.8 Hz, $J_{C,P}$ = 3.9 Hz, *C*-tazdt), 143.3 (dd, $^3J_{C,P}$ = 12.3 Hz, $J_{C,P}$ = 3.7 Hz, *C*-tazdt), 133.9 (dd, $^3J_{C,P}$ = 11.4 Hz, $J_{C,P}$ = 7.0 Hz, *C*-Ph), 132.1 (d, $J_{C,P}$ = 2.4 Hz, *C*-Ph), 130.7–129.9 (m, *C*-Ph), 129.4 (s, *C*-(2,4-dMOB)), 129.3 (dd, $^2J_{C,P}$ = 10.7 Hz, $J_{C,P}$ = 7.3 Hz, *C*-Ph), 117.3 (s, *C*-(2,4-dMOB)), 104.8 (s, *C*-(2,4-dMOB)), 98.4 (s, *C*-(2,4-dMOB)), 55.6 (s, CH_3), 55.3 (s, CH_3), 44.6 (s, NCH_2), 28.2–27.5 (m, CH_2-dppe). ^{31}P NMR (DMF-D_7, δ, ppm, 122 MHz, 298 K): 58.4 (d, $^3J_{P,P}$ = 18.0 Hz, *P*-dppe), 56.1 (d, $^3J_{P,P}$ = 18.0 Hz, *P*-dppe). MS (ESI-TOF, 9:1 MeOH:H_2O with 0.1% HCOOH, *m*/*z*): 786 (M + H^+). IR (CH_2Cl_2, $\tilde{\nu}$, cm^{-1}): 3043 (w), 1647 (m), 1437 (m), 1259 (s), 739 (s), 705 (s).

2.2.3. Synthesis of [(dppe)Pt(5b)] (**8**)

In a 50 mL Schlenk flask [(dppe)$PtCl_2$] (0.088 g, 1.326 mmol) was dissolved in MeOH (10 mL). A solution of **5b** (0.042 g, approx. 1.484 mmol) and KOH (0.017 g, 0.303 mmol) in MeOH (10 mL) was added. The yellow suspension was diluted with CH_2Cl_2 (15 mL) and stirred for 3 days at room temperature. After drying in vacuo the purification was carried out chromatographically with a CH_2Cl_2/MeOH solvent mixture (20/1) as mobile phase. Crystals suitable for X-ray structural analysis were obtained from a saturated CH_2Cl_2 solution with *n*-pentane: yield 0.088 g (75%). ^{1}H NMR (CD_2Cl_2, δ, ppm, 300 MHz, 298 K): 7.85–7.75 (m, 8 H, *H*-Ph), 7.52–7.49 (m, 12 H, *H*-Ph), 6.87 (d, $^3J_{H,H}$ = 8.3 Hz, 1 H, *H-o*-(2,4-dMOB)), 6.40 (d, $J_{H,H}$ = 2.4 Hz, 1 H, *H-m'*-(2,4-dMOB)), 6.33 (dd, $^3J_{H,H}$ = 8.3 Hz, $J_{H,H}$ = 2.4 Hz, 1 H, *H-m*-(2,4-dMOB)), 5.18 (s, 2 H, NCH_2), 3.75 (s, 3 H, CH_3), 3.70 (s, 3 H, CH_3), 2.51–2.45 (m, 4 H, CH_2-dppe). ^{13}C NMR (CD_2Cl_2, δ, ppm, 75 MHz, 298 K): 161.0 (s, *C*-(2,4-dMOB)), 158.3 (s, *C*-(2,4-dMOB)), 134.0 (dd, $^2J_{C,P}$ = 11.0 Hz, $J_{C,P}$ = 1.1 Hz, *C*-Ph), 132.3–132.2 (m, *C*-Ph), 130.0 (s, *C*-(2,4-dMOB)), 129.2 (dd, $^2J_{C,P}$ = 11.0 Hz, $J_{C,P}$ = 2.4 Hz, *C*-Ph), 117.3 (s, *C*-(2,4-dMOB)), 104.5 (s, *C*-(2,4-dMOB)), 98.6 (s, *C*-(2,4-dMOB)), 55.8 (s, CH_3),

55.7 (s, CH_3), 45.8 (s, NCH_2), 29.4–28.6 (m, CH_2-dppe). ^{31}P NMR (CD_2Cl_2, δ, ppm, 122 MHz, 298 K): 45.7 (d, $^3J_{P,P}$ = 10.3 Hz, *P*-dppe, Pt-satellites: dd, $^1J_{P,Pt}$ = 2854.1 Hz, $^3J_{P,P}$ = 10.3 Hz), 45.4 (d, $^3J_{P,P}$ = 10.3 Hz, *P*-dppe, Pt-satellites: dd, $^1J_{P,Pt}$ = 2782.8 Hz, $^3J_{P,P}$ = 10.3 Hz). MS (ESI-TOF, 9:1 MeOH:H_2O with 0.1% HCOOH, *m*/*z*): 874.1354 (M + H^+). IR (CH_2Cl_2, $\tilde{\nu}$, cm^{-1}): 3049 (w), 1437 (m), 1269 (s), 1105 (w), 748 (s), 721 (s), 533 (m).

2.2.4. General Synthesis of **9**

In a 50 mL Schlenk flask 1 equivalent [$(PPh_3)_2PtCl_2$] was suspended in MeOH (10 mL). A solution of 1.1 equivalents **5a**–**c** and 3 equivalents NaOMe in MeOH (10 mL) and CH_2Cl_2 (10 mL) was added. After stirring for 3 days at room temperature, the clear yellow solution was dried in vacuo and purified by column chromatography with CH_2Cl_2/MeOH solvent mixture (20/1) as mobile phase. Crystals suitable for X-ray structural analysis were obtained from a saturated CH_2Cl_2 solution with *n*-pentane.

[$(PPh_3)_2$Pt(**5a**)] (**9a**) and (**12**), 0.207 g (0.26 mmol) [$(PPh_3)_2PtCl_2$], 0.034 g (0.63 mmol) NaOMe, 0.074 g (approx. 0.30 mmol) **5a**: yield 0.088 g (76%, **9a**). **12** could be isolated from the first fraction of the same chromatography. ^{1}H NMR (CD_2Cl_2, δ, ppm, 500 MHz, 298 K): 7.50–7.47 (m, 13 H, *H*-Ph), 7.38–7.35 (m, 4 H, *H*-Ph), 7.24–7.18 (m, 13 H, *H*-Ph), 7.10 (d, $^3J_{H,H}$ = 8.7 Hz, 2 H, *H*-*o*-(4-MOB)), 6.76 (d, $^3J_{H,H}$ = 8.7 Hz, 2 H, *H*-*m*-(4-MOB)), 4.99 (s, 2 H, NCH_2), 3.78 (s, 3 H, CH_3). ^{13}C NMR (CD_2Cl_2, δ, ppm, 125 MHz, 298 K): 159.7 (s, *C*-(4-MOB)), 154.7 (d, $^3J_{C,P}$ = 10.8 Hz, *C*-tazdt), 142.7 (d, $^3J_{C,P}$ = 12.0 Hz, *C*-tazdt), 135.4 (dd, $^3J_{C,P}$ = 8.3 Hz, $J_{C,P}$ = 1.9 Hz, *C*-Ph), 131.2 (dd, $J_{C,P}$ = 3.6 Hz, $J_{C,P}$ = 1.9 Hz, *C*-Ph), 130.4 (s, *C*-(4-MOB)) 130.3 (dd, $^1J_{C,P}$ = 59.0 Hz, $^3J_{C,P}$ = 9.2 Hz, *C*-Ph), 128.1 (dd, $^2J_{C,P}$ = 11.1 Hz, $J_{C,P}$ = 4.5 Hz, *C*-Ph), 114.0 (s, *C*-(4-MOB)), 55.6 (s, CH_3), 51.0 (s, CH_2). ^{31}P NMR (CD_2Cl_2, δ, ppm, 202 MHz, 298 K): 17.2 (d, $^3J_{P,P}$ = 21.0 Hz, *P*-dppe, Pt-satellites: dd, $^1J_{P,Pt}$ = 2914.9 Hz, $^3J_{P,Pt}$ = 20.8 Hz), 17.1 (d, $^3J_{P,P}$ = 21.0 Hz, *P*-dppe, Pt-satellites: dd, $^1J_{P,Pt}$ = 2943.3 Hz, $^3J_{P,Pt}$ = 20.8 Hz). IR (CH_2Cl_2, $\tilde{\nu}$, cm^{-1}): 1436 (m), 1259 (s), 1094 (m), 738 (s), 708 (s), 525 (m).

[$(PPh_3)_2$Pt(**5b**)] (**9b**), 0.192 g (0.24 mmol) [$(PPh_3)_2PtCl_2$], 0.046 g (0.85 mmol) NaOMe, 0.069 g (approx. 0.24 mmol) **5b**: yield 0.103 g (42%). Anal. Calcd. for $C_{47}H_{41}N_3O_2P_2PtS_2$: C, 56.39; H, 4.13; N, 4.20; S, 6.41%. Found: C, 56.66; H, 4.27; N, 4.27; S, 6.63%. ^{1}H NMR (CD_2Cl_2, δ, ppm, 500 MHz, 298 K): 7.53–7.43 (m, 12 H, *H*-Ph), 7.38–7.34 (m, 6 H, *H*-Ph), 7.23–7.18 (m, 12 H, *H*-Ph), 6.86 (dd, $^3J_{H,H}$ = 7.98 Hz, $J_{H,H}$ = 0.56 Hz, 1 H, *H*-*o*-(2,4-dMOB)), 6.36 (t, $J_{H,H}$ = 2.41 Hz, 1 H, *H*-*m*-(2,4-dMOB)), 6.33 (d, $J_{H,H}$ = 2.41 Hz, 1 H, *H*-*m*′-(2,4-dMOB)), 5.03 (s, 2 H, NCH_2), 3.78 (s, 3 H, CH_3), 3.65 (s, 3 H, CH_3). ^{13}C NMR (CD_2Cl_2, δ, ppm, 125 MHz, 298 K): 161.0 (s, *C*-(2,4-dMOB)), 158.5 (s, *C*-(2,4-dMOB)), 154.2 (dd, $^3J_{C,P}$ = 14.2 Hz, $J_{C,P}$ = 3.2 Hz, *C*-tazdt), 143.3 (dd, $^3J_{C,P}$ = 16.0 Hz, $J_{C,P}$ = 3.6 Hz, *C*-tazdt), 135.4 (t, $J_{C,P}$ = 10.8 Hz, *C*-Ph), 131.2 (dd, $J_{C,P}$ = 12.3 Hz, $J_{C,P}$ = 2.4 Hz, *C*-Ph), 130.8 (s, *C*-(2,4-dMOB)), 130.4 (ddd, $^1J_{C,P}$ = 56.4 Hz, $^3J_{C,P}$ = 29.3 Hz, $J_{C,P}$ = 1.7 Hz, *C*-Ph), 128.1 (d, $^2J_{C,P}$ = 11.1 Hz, *C*-Ph), 117.0 (s, *C*-(2,4-dMOB)), 104.5 (s, *C*-(2,4-dMOB)), 98.5 (s, *C*-(2,4-dMOB)), 55.8 (s, CH_3), 55.7 (s, CH_3), 45.5 (s, NCH_2). ^{31}P NMR (CD_2Cl_2, δ, ppm, 202 MHz, 298 K): 17.7 (d, $^3J_{P,P}$ = 21.0 Hz, *P*-dppe, Pt-satellites: dd, $^1J_{P,Pt}$ = 2996.7 Hz, $^3J_{P,Pt}$ = 20.8 Hz), 16.7 (d, $^3J_{P,P}$ = 21.0 Hz, *P*-dppe, Pt-satellites: dd, $^1J_{P,Pt}$ = 2835.2 Hz, $^3J_{P,Pt}$ = 20.8 Hz). IR (CH_2Cl_2, $\tilde{\nu}$, cm^{-1}): 3055 (m), 1437 (m), 1268 (s), 1094 (w), 738 (s), 710 (s), 526 (m).

[$(PPh_3)_2$Pt(**5c**)] (**9c**), 0.260 g (0.33 mmol) [$(PPh_3)_2PtCl_2$], 0.067 g (1.24 mmol) NaOMe, 0.080 g (approx. 0.34 mmol) **5c**: yield 0.238 g (80%). Anal. Calcd. for $C_{43}H_{43}N_3P_2PtS_2Si$: C, 54.30; H, 4.56; N, 4.42; S, 6.74%. Found: C, 54.37; H, 4.39; N, 4.29; S, 6.43%. ^{1}H NMR (CD_2Cl_2, δ, ppm, 500 MHz, 298 K): 7.53–7.47 (m, 12 H, *H*-Ph), 7.37–7.34 (m, 6 H, *H*-Ph), 7.23–7.19 (m, 12 H, *H*-Ph), 3.96–3.92 (m, 2 H, NCH_2), 1.05–1.01 (m, 2 H, CH_2TMS), −0.06 (s, 9 H, CH_3-TMS). ^{13}C NMR (CD_2Cl_2, δ, ppm, 125 MHz, 298 K): 154.5 (dd, $^3J_{C,P}$ = 13.7 Hz, $J_{C,P}$ = 3.1 Hz, *C*-tazdt), 142.1 (dd, $^3J_{C,P}$ = 15.9 Hz, $J_{C,P}$ = 3.0 Hz, *C*-tazdt), 135.4 (dd, $J_{C,P}$ = 10.7 Hz, $J_{C,P}$ = 6.2 Hz, *C*-Ph), 131.2 (s, *C*-Ph), 130.6 (s, *C*-Ph), 128.1 (dd, $^2J_{C,P}$ = 10.7 Hz, $J_{C,P}$ = 5.5 Hz, *C*-Ph), 44.4 (s, NCH_2), 17.8 (s, CH_2TMS), -1.8 (s, CH_3-TMS). ^{31}P NMR (CD_2Cl_2, δ, ppm, 202 MHz, 298 K): 17.4 (d, $^3J_{P,P}$ = 21.0 Hz, *P*-dppe, Pt-satellites: dd, $^1J_{P,Pt}$ = 2861.0 Hz, $^3J_{P,Pt}$ = 20.9 Hz), 16.9 (d, $^3J_{P,P}$ = 21.0 Hz, *P*-dppe, Pt-satellites: dd, $^1J_{P,Pt}$ = 2988.1 Hz,

$^3J_{P,Pt}$ = 20.9 Hz). ^{29}Si-NMR (CD_2Cl_2, δ, ppm, 99 MHz, 298 K): 0.6–0.1 (m, *Si*-TMS). IR (CH_2Cl_2, $\tilde{\nu}$, cm^{-1}): 3056 (w), 2967 (w), 1437 (m), 1259 (s), 1094 (m), 724 (s), 526 (m).

2.2.5. Synthesis of **10**

In a 50 mL Schlenk flask, **5c** (0.081 g, approx. 0.35 mmol) were dissolved in THF (50 mL). Next, [(η^5-C_5H_5)Co(CO)I_2] (0.142 g, 0.35 mmol) and NEt_3 (0.11 mL, 0.76 mmol) were added to the solution. The blue solution was stirred for 4 days at room temperature. The purification was carried out chromatographically with a CH_2Cl_2/MeOH solvent mixture (20/1) as mobile phase. Crystals suitable for X-ray structural analysis were obtained from a saturated CH_2Cl_2 solution with *n*-pentane: yield 0.053 g (43%). ^{1}H NMR (dimer, $CDCl_3$, δ, ppm, 500 MHz, 298 K): 4.80 (s, 5 H, *H*-Cp), 4.42–4.30 (m, 2 H, NCH_2), 1.49–1.33 (m, 2 H, CH_2TMS), 0.16 (s, 9 H, CH_3-TMS). ^{13}C NMR (dimer, $CDCl_3$, δ, ppm, 125 MHz, 298 K): 156.0 (*C*-tazdt), 151.2 (*C*-tazdt), 88.7 (*C*-Cp), 45.7 (NCH_2), 18.1 (CH_2TMS), −1.6 (CH_3-TMS). ^{29}Si NMR (dimer, $CDCl_3$, δ, ppm, 99 MHz, 298 K): 1.1–0.4 (m, *Si*-TMS). MS (ESI-TOF, 9:1 MeOH:H_2O with 0.1% HCOOH, *m*/*z*): 356 (M + H^+), 710 (M_2). IR (CH_2Cl_2, $\tilde{\nu}$, cm^{-1}): 2968 (w), 2879 (w), 1483 (w), 1267 (s), 846 (s), 748 (s), 708 (s), 558 (m).

2.2.6. Synthesis of **11**

In a 50 mL Schlenk flask, a solution of **5a** (0.103 g, approx. 0.41 mmol) in THF (30 mL) was treated with [(η^5-C_5H_5)Co(CO)I_2] (0.165 g, 0.41 mmol) and NEt_3 (0.12 mL, 0.90 mmol). The blue solution was stirred for 5 days at room temperature. The purification was carried out chromatographically with a CH_2Cl_2/MeOH solvent mixture (20/1). Compound **11** was isolated from the first blue fraction. Crystals suitable for X-ray structural analysis were obtained from a saturated CH_2Cl_2 solution with *n*-pentane. Yield: 0.008 g (1%).

3. Results and Discussion

3.1. Ligand Synthesis

In contrast to the [3 + 2] cyclization reaction using bis(sulfanyl)acetylene described in a recent publication, mono(sulfanyl)ethyne was used to check whether an insertion of the second benzylsulfanyl group is more advantageous at the cyclized triazole than at the alkyne [16]. The synthesis of the sulfur-substituted triazole derivatives **1a**–**g** was carried out by a CuAAC reaction with an azide bearing the N-protective groups 4-methoxybenzyl (4-MOB), 2,4-dimethoxybenzyl (2,4-dMOB), 3,4-dimethoxybenzyl (3,4-dMOB), 2-(trimethylsilyl)ethyl (TMS-C_2H_4), 2,6-dimethylphenyl (Xy), benzyl (Bn) or 2-picolyl (2-Pic) and benzylsulfanylacetylene (Scheme 1, Table 1). Simply, $CuSO_4 \cdot 5\ H_2O$ was used here as the catalyst system, which was reacted in situ with sodium ascorbate (NaAsc) to obtain the catalytically active Cu^I (Scheme 1) [5,10,22,23].

After purification by column chromatography, the N-protected 1*H*-1,2,3-triazole-4-monosulfides were isolated in yields of 36% to 97% (Table 1) and were characterized by NMR spectroscopy. It should be noted that the regioselective cyclization led exclusively to the 4-sulfido derivative, which is in accord with observations of Meldal and Sharpless. [5,24] The introduction of the second sulfur substituent is carried out analogously to synthesis of bis(benzylsulfanyl)acetylene described in the literature. [25] For this purpose, the corresponding triazoles **1a**–**g** were deprotonated with *n*-butyllithium at −78 °C, reacted with elemental sulfur and subsequently trapped with benzyl bromide (Scheme 1). After purification by column chromatography, the corresponding triazoles **2a**–**e** were isolated in yields between 38% and 89% (Table 1).

In the ^{1}H NMR spectra, 2 new signals were observed at a chemical shift between 3.55 ppm and 3.79 ppm for the CH_2 protons of the introduced benzyl group, while the triazole proton of **1a**–**g** between 7.05 ppm and 7.68 ppm had disappeared (Figures S32–S46). In the case of compound **1g**, the introduction of sulfur at 5-position failed.

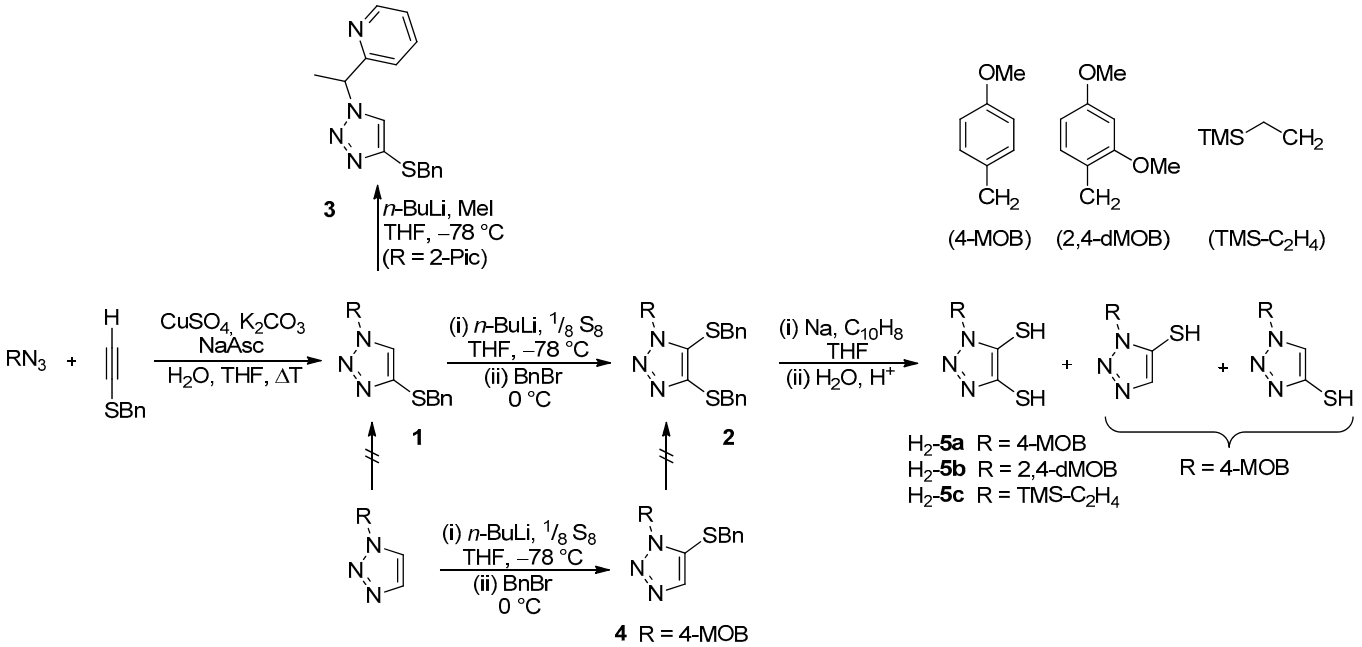

Scheme 1. CuAAC reaction to build 4-benzylsulfanyl-1*H*-1,2,3-triazole, subsequent introduction of a second sulfide group and reductive removal of the S-benzyl groups to form the free dithiol derivatives.

Table 1. List of N-protective groups and respective yields with regard to Scheme 1 (The letters in column 1 refer to the different *N*-R triazole derivatives in Scheme 1).

	R		1	2
a	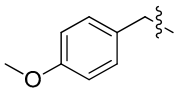	4-MOB	97%	76%
b	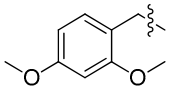	2,4-dMOB	83%	89%
c	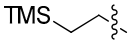	TMS-C_2H_4	93%	48%
d	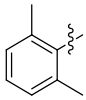	Xy	49%	38%
e	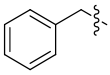	Bn	80%	65%
f	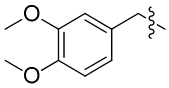	3,4-dMOB	36%	76%
g	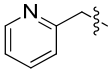	2-Pic	91%	-

Due to the electron-withdrawing pyridine substituent in the 2-picolyl protective group, the acidity of the methylene proton is higher than that of the triazole proton. Accordingly, deprotonation and subsequent methylation with MeI occurs at the N-2-picolyl group to give **3**, as can be observed by the doublet ^{1}H NMR signal at 1.88 ppm for the methyl group attached to the N-protective group (Figure S49). Also in a [3 + 2] cycloaddition of bis(benzylsulfanyl)acetylene and 2-picolyl azide with $CuSO_4$/NaAsc as catalyst **2a** was not isolated. A terminal acetylene is necessary for an end-on coordination of the Cu^I to catalyze the [3 + 2] cycloaddition [10].

Nevertheless, this new two-step method for the generation of a disulfide unit on the 1*H*-1,2,3-triazole shows clear advantages in comparison with the synthesis described in the literature. Thus, sensitive and expensive catalyst systems [(NHC)CuI] and [(η^5-C_5Me_5)(cod)RuCl] are dispensable [16]. Moreover, anaerobic and anhydrous conditions are not necessary in the first reaction steps and the overall yields are higher. While Schallenberg et al. achieved a yield of 39% with the benzyl group, a yield of 65% was realized with the new route [16]. Accordingly, it was also investigated whether the disulfide unit can be introduced stepwise into a 1,2,3-triazole by the direct method. For this purpose, the unsubstituted 1-(4-methoxybenzyl)-1*H*-1,2,3-triazole was deprotonated with *n*-butyllithium and subsequently reacted with elemental sulfur and benzyl bromide for alkylation (Scheme 1). After chromatographic purification, the ^{1}H NMR spectrum of the isolated product **4** revealed a methylene singlet at 3.67 ppm and a triazole proton at 7.48 ppm, indicating introduction of the sulfur in 5- instead of 4-position (Figure S52). Interestingly, a preference for the 5-substituted derivatives was also observed by Fokin et al. by ruthenium-catalyzed [3 + 2] cycloadditions of terminal alkynes with azides [26–28]. The regioselective deprotonation can be explained by the greater stabilization of the carbanion in 5-position due to resonance (Figure 1). Consistently, a subsequent introduction of the second sulfur substituent at 4-position by the same procedure proved unsuccessful. Respective attempts always led to the recovery of the starting material, which can be attributed to a lack of resonance stabilization in the carbanion.

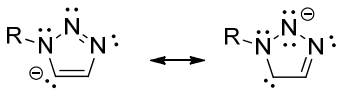

Figure 1. Mesomeric structures after deprotonation.

To enable coordination via dithiolene unit, the benzyl protective groups on sulfur must be removed. Due to having the best yields, compounds **2a**–**c** were used for coordination experiments. As we previously reported, this could readily be achieved by reductive removal with elemental sodium in presence of naphthalene in THF [16]. After an acidic work-up, the corresponding dithiols **5a**–**c** were isolated as yellow oils in reasonable yields (Scheme 1). The samples are not analytically but sufficiently pure for coordination experiments (*vide infra*).

3.2. Synthesis of Metal Complexes

Coordination experiments with 1*H*-1,2,3-triazoles-4,5-dithiols were performed with particular attention to the regioselective dithiolate over N-coordination. The dithiols H_2-**5a**–**c** were reacted with the first-row and group-10 transition metals Co^{III}, Ni^{II}, Pd^{II} and Pt^{II}. The Co^{III} complex **10** was synthesized by reacting the ligand H_2-**5c** with [(η^5-C_5H_5)Co(CO)I_2] in THF in presence of NEt_3 (Scheme 2). The reaction progress could be observed by a decrease of the CO band in IR spectroscopy and the reaction solution turning blue.

In contrast to the free dithiol H_2-**5c**, the corresponding complex could be purified by flash chromatography, such that a dark purple compound was isolated and identified as the Co-complex **10**. Further, the dppe-complexes **6** and **7** with group-10 metals were obtained either by reaction of H_2-**5b** in a two-phase system (CH_2Cl_2/H_2O) with KOH and the precursors [(dppe)MCl_2] {M = Ni, Pd; dppe = 1,2-bis(diphenylphosphino)ethane} or with [(dppe)$PtCl_2$] and [$(PPh_3)_2PtCl_2$], respectively, in MeOH using NaOMe as a base. After aqueous work-up and chromatographic purification, a green Ni compound (**6**), a reddish Pd compound (**7**) and yellow Pt compounds (**8** and **9a**–**c**) were isolated.

In addition to the main products, by-products were surprisingly isolated from the reaction mixtures with the crude dithiol H_2-**5a** and corresponding metal precursors (Scheme 3). From the reaction with [(η^5-C_5H_5)Co(CO)I_2], a tetranuclear complex **11** and from the reaction with [$(PPh_3)_2PtCl_2$] the by-product **12** were isolated and crystallized.

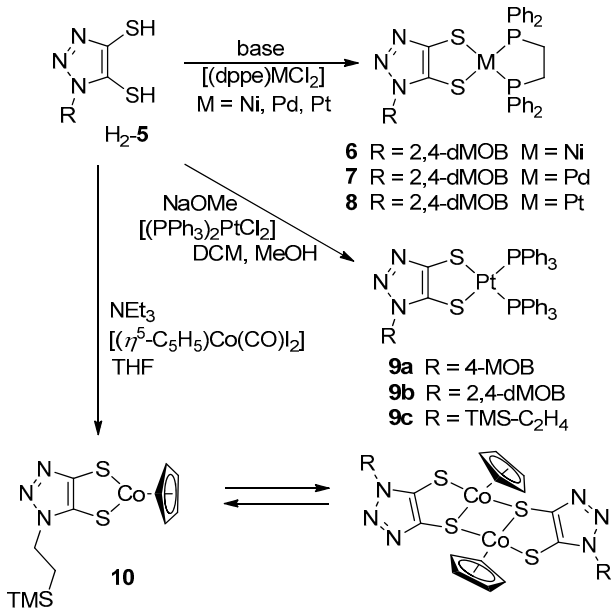

Scheme 2. Coordination of 5^{2-} at Ni^{II} (**6**), Pd^{II} (**7**), Pt^{II} (**8**) and Co^{III} (**10**) (base = KOH or NaOMe).

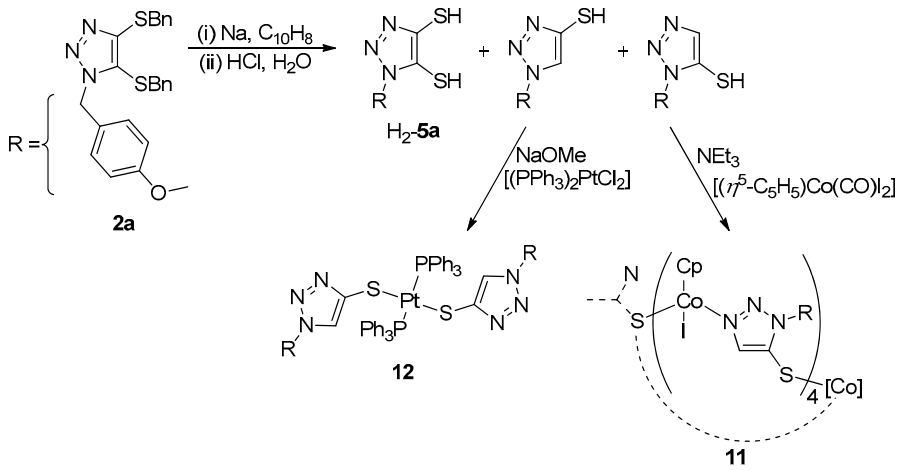

Scheme 3. Coordination to by-products **11** and **12**.

3.3. Molecular Structure of the Complexes

The molecular structures of all complexes **6**–**12** were determined by single-crystal XRD analysis (Figures 2, 3, S4 and S5). With the exception of the complexes **11** and **12**, which are by-products, all complexes exhibited an exclusive dithiolato coordination. The molecular structures of the group-10 metals showed the expected square planar geometry, including a planar dithiolate unit. The deviation from the SCCS planarity fell between 1.0(5)° and 3.1(3)°, which is very much in accordance with the values described in the literature [29]. Table 2 lists selected bond lengths and angles. In comparison to classical dithiolene complexes, a larger obtuse bite angle and, related to that, somewhat longer metal–sulfur bonds are evident [30–33]. The former follows the geometric requirements of a five-membered backbone ring, in which a regular internal angle leads to a formal C–C–S angle of 126°. In addition, comparison of the metric parameters in compounds **9a** and **9b** does not show any influence by the protective group on nitrogen in the bonding situation at the dithiolate unit.

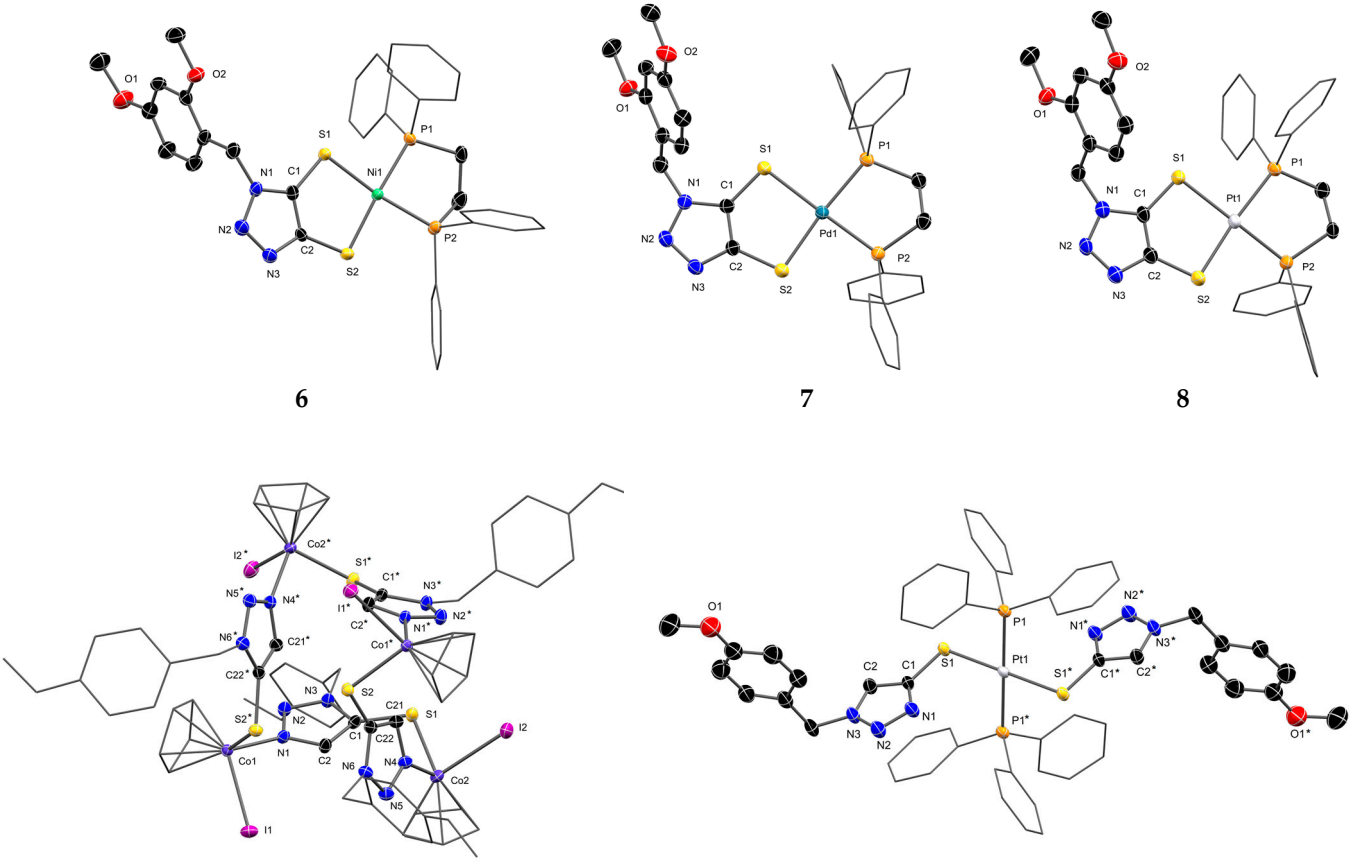

6 **7** **8**

11 **12**

Figure 2. Molecular structure of **6**–**8**, **11** and **12** in the crystal with ellipsoids set at 50% probability. Hydrogen atoms have been omitted for clarity and phenyl or 4-methoxybenzyl (**11**) substituents are displayed as wireframe.

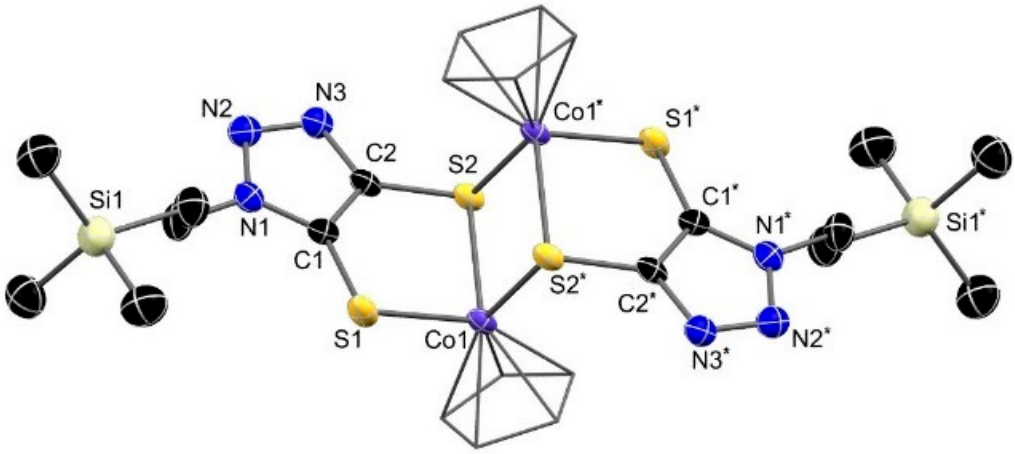

Figure 3. Molecular structure of the dimer **10** in the crystal with ellipsoids set at 50% probability. Hydrogen atoms have been omitted for clarity and η^5-C_5H_5 rings are displayed as wireframe.

Table 2. Comparison of essential bond lengths [Å] and bite angles [°].

	C–S	C–S	C–C	M–S1	M–S2/M–S2*	S1–M–S2
6	1.726(4)	1.747(4)	1.368(6)	2.199(1)	2.187(1)	95.80(4)
[(dppe)Ni(tazdt-Bn)] [16]	1.719(3)	1.750(3)	1.370(4)	2.1982(8)	2.1925(8)	96.09(3)
7	1.725(5)	1.748(6)	1.381(5)	2.354(2)	2.334(1)	92.99(5)
[(dppe)Pd(tazdt-Bn)] [16]	1.7333(15)	1.7400(17)	1.377(2)	2.3475(4)	2.3397(4)	92.90(1)
8	1.741(6)	1.736(4)	1.369(5)	2.349(1)	2.335(1)	92.15(4)
[(dppe)Pt(dmit)] [34]	1.710(11)	1.716(11)	1.366(16)	2.315(3)	2.308(3)	90.0(1)
[(dppe)Pt(dddt)] [35]	-	-	-	2.3157(13)	2.3235(15)	88.25(5)
9a	1.724(3)	1.739(3)	1.373(3)	2.3344(7)	2.3487(7)	90.82(2)
9b	1.725(5)	1.752(3)	1.369(6)	2.3536(9)	2.336(1)	91.08(4)
$[(PPh_3)_2Pt(dmit)]$ [36]	1.722(4)	1.750(4)	1.349(6)	2.3319(11)	2.3192(11)	89.22(4)
10	1.718(5)	1.751(7)	1.380(8)	2.278(2)	2.271(1)/2.269(1)	93.81(5)
$[(\eta^5\text{-}C_5H_5)Co(Cl_3bdt)]$ [33]	1.734(11)	1.765(11)	1.384(18)	2.211(2)	2.214(3)/2.270(3)	89.61(12)
$[(\eta^5\text{-}C_5H_5)Co(bdt)]$ [32]	1.757(4)	1.783(3)	1.382	2.246(1)	2.230(1)/2.272(1)	89.73(4)
11	1.739(2)	1.739(2)	1.739(2)/1.379(3)	2.2601(7)	2.2721(6)	-
12	1.747(3)		1.379(4)	2.3274(7)		-

dddt = 5,6-dihydro-1,4-dithiin-2,3-dithiolate; dmit = 1,3-dithiole-2-thione-4,5-dithiolate.

Moreover, when replacing the metal center from Ni^{II} (**6**) to Pd^{II} (**7**) or Pt^{II} (**8**), the dithiolate moiety does not show significant differences in the bond lengths C1–C2 with 1.368(6) Å to 1.381(5) Å or C1–S1 and C2–S2, which are between 1.725(5) Å and 1.748(6) Å. On the other hand, the M–S bond lengths show a distinct elongation by going from Ni^{II} to Pd^{II} and Pt^{II}, which is essentially related to the increasing size of the metal atom. However, the bond lengths Pd–S in **7** {2.354(2) Å and 2.334(1) Å} and Pt–S in **8** {2.349(1) Å and 2.335(1) Å} are virtually equal. This effect is well-known and is attributed to the relativistic effect of the Pt atom and the resulting shrinking of the *d* orbitals [34].

The molecular structure of **10** in the solid state reveals a dimerization, in which not only is the Co^{III} center coordinated by one dithiolate unit, but a third sulfur atom of a neighboring dithiolate moiety is bound to cobalt and vice versa. The observed dimerization to $(\mathbf{10})_2$ can be rationalized by fulfilling the 18 valence electron rule. On the other hand, the monomer constitutes a 16 valence electron complex, which is less stable but more readily solvated due to the free coordination site. Such dimerization equilibria are regularly observed in related $[(\eta^5\text{-}C_5H_5)Co(\text{dithiolene})]$ complexes [32,33,37–40].

If the $\eta^5\text{-}C_5H_5$ ring is considered as occupying a single coordination site, the Co^{III} centers show a τ-parameter of 0.76, which is close to $\tau = 1$ of a tetrahedron [41]. The bond length M–S2* of 2.269(1) Å is comparable to that of M–S1 {2.278(2) Å} and M–S2 {2.271(1) Å}. In studies on the compounds $[CpCo(Cl_3bdt)]_2$ and $[CpCo(bdt)]_2$ (bdt = benzene-1,2-dithiolate), the Co-S bond lengths fall between 2.211(2) Å and 2.246(1) Å and are again slightly shorter than the bond lengths determined in **10**. [32,33] Accordingly, as described in the literature, the distance between the Co centers between 3.212(6) Å and 3.2893(4) Å is slightly shorter than the distance determined in **10** with 3.3055(9) Å. None correspond to a direct Co-Co bond of 2.32 Å. [21].

A by-product of the reaction of H_2-**5a** with $[(\eta^5\text{-}C_5H_5)Co(CO)I_2]$ was isolated after chromatography and crystallization. The crystal structure of **11** undisclosed an unexpected tetranuclear complex, in which the Co^{III} ions are linked in a cyclic fashion by N-4-methoxybenzyl-1,2,3-tiazole-5-thiolate ligands (Figure 2). Herein, each Co^{III} is coordinated by a thiolate of one triazole and by a nitrogen atom in the third position of another. The coordination sphere of each Co^{III} center is saturated by one iodide and one $\eta^5\text{-}C_5H_5$ ligand. This structural motif uncovered the loss of one thiolate substituent at 4-position of the 1,2,3-triazole ligand.

Likewise, the triazole ligands in the by-product **12** do not contain a dithiolate unit. Instead, the two triazole ligands in **12**, next to two trans-standing triphenylphosphine ligands, are coordinated via one remaining thiolate in 4-position in a quadratic planar geometry around a Pt^{II} center. A comparison of complex **12** with **9a** with respect to the influence of cis/trans configuration is interesting, because the ligands are highly similar. The *trans* arrangement leads to longer Pt–P1/P1* bonds (2.3220(8) Å) in **12** compared to the *cis* arrangement in **9a** with Pt–P1/P2: 2.2853(7) Å/2.2944(7) Å, which reflects some symbiotic π-bonding effect in **9a**. The successful isolation of low-yield by-products **11** and **12** indicate limitation of side reactions in the reductive removal of the thiol protective groups. Remarkably, the cleavage of the whole benzylthiolate is possible both at 4- and 5-position.

3.4. NMR Spectroscopy of Metal Complexes

The phosphine ligands in the complexes **6**–**8** and **9a**–**c** are valuable probes for the electronic situation of the metal, which can be investigated by ^{31}P NMR spectroscopy. The Ni complex **6** as well as the Pd compound **7** show two doublets at chemical shifts of 58.7/60.5 ppm, and 56.1/58.4 ppm, respectively. The observed doublets result from the C_1 symmetry and the related chemical non-equivalence of the phosphorus atoms. Consistently, a slightly smaller coordination chemical shift $\Delta\delta$ of the Pd-dppe signals is combined with a lower $^{31}P/^{31}P$ coupling constant of 18.0 Hz. The Ni-dppe complex **6** shows a substantially larger coupling constant of 47.9 Hz. The doublet signals for the corresponding Pt^{II} compound **8** were detected at 45.4 ppm and 45.7 ppm, with a coupling constant of 10.5 Hz confirming the trend $J_{P,P}$(Ni) > $J_{P,P}$(Pd) > $J_{P,P}$(Pt) and δ(Ni) > δ(Pd) > δ(Pt). Related observations were already reported for [(dppe)M(mnt)] (mnt = maleonitriledithiolate) serving as a selected example [29].

With the change of the ligand dppe to PPh_3 in compounds **9a**–**c**, two doublets are observed at the chemical shift between 16.7 ppm and 17.7 ppm. In addition to the $^{31}P/^{31}P$ coupling ($J_{P,P}$ = 21.0 Hz), $^{31}P/^{195}Pt$ coupling constants between 2861 Hz and 2998 Hz are observed (Table 3), which are in good agreement with other dithiolene-Pt compounds [31,42,43].

Table 3. Chemical shifts in ^{31}P NMR spectroscopy and the respective coupling constants.

	M	δ **[ppm]**	$J_{P,P}$ **[Hz]**	$J_{P,Pt}$ **[Hz]**
6	Ni	60.5/58.7	47.9	-
7	Pd	58.4/56.1	18.0	-
8	Pt	45.7/45.4	10.5	2778/2760
9a	Pt	17.2/17.1	21.0	2915/2943
9b	Pt	17.7/16.7	21.0	2862/2998
9c	Pt	17.4/16.9	21.0	2861/2988

Here, the PPh_3 is particularly well-suited for observing changes in the electronic situation of the complex by means of ^{31}P-NMR spectroscopy [42]. The individual N-protective group in **9a**–**c** exerts only a minor influence on the $^{31}P/^{195}Pt$ coupling constant. However, the slightly differing trans effect of the asymmetric dithiolate on the phosphines is reflected in the variance of the $^{31}P/^{193}Pt$ coupling constant, spanning ΔJ range from 28 Hz (**9a**) to 136 Hz (**9b**).

3.5. Electronic Structure Elucidation

The different electronic situation in compounds **6**–**8** is revealed by UV/Vis spectroscopy and cyclic voltammetry. Figure 4 shows the UV/Vis spectra of compounds **6**, **7** and **8**. In the visible range between 400 and 700 nm characteristic absorption bands at 409 nm (**8**), 523 nm (**7**) and 602 nm (**6**) are observed, which are responsible for the characteristic color of the compounds: green (**6**), red (**7**) and yellow (**8**). According to TD-DFT calculations, the underlying excitation can be assigned to a dithiolate-π to metal-d transition. Hence, the trend **6** > **7** > **8** in λ reflect the increasing ligand field splitting in the

order Ni, Pd, Pt. Consistently, in cyclic voltammetry, a reduction process requires lower potentials for heavier metals. The Ni compound **6** shows a reversible Ni^{II}/Ni^{I} reduction with a half-step potential of −1.79 V, while an irreversible signal at a potentials of −2.14 V and −2.60 V, respectively, are observed for complexes **7** and **8**. DFT calculations on related Ni and Pd dppe complexes of N-2,6-dimethylphenyltriazole-4,5-dithiolate and the corresponding anions resulted that the reversible reduction $Ni^{II,I}$ is based on a substantial distortion to tetrahedral, which is not relevant for Pd and Pt. Accordingly, the calculated ΔG value for the reduction are higher for Pd and Pt compared with Ni. [16].

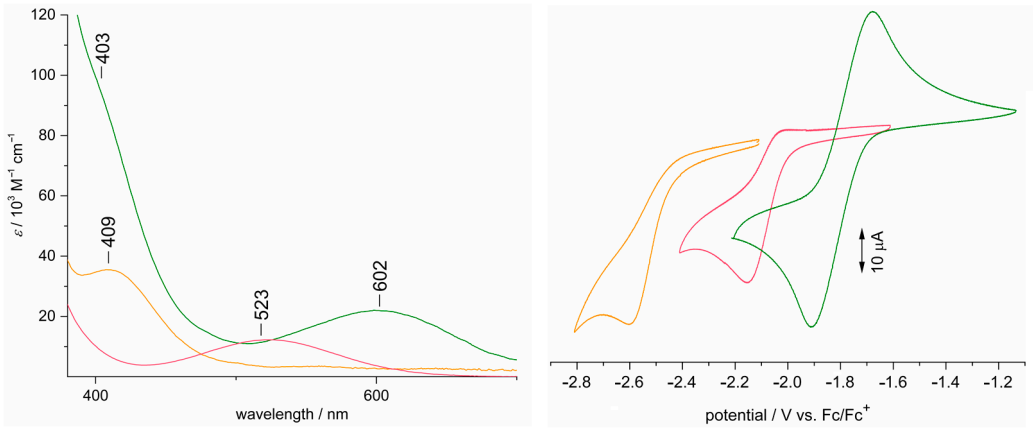

Figure 4. UV/Vis spectra (CH_2Cl_2, **left**) and cyclic voltammetry (CH_2Cl_2 or DMF, **right**) of the compounds **6** (green), **7** (red) and **8** (yellow).

3.6. Investigation of Dimerization

The dimerization of complex **10** to form $(\mathbf{10})_2$ found in the solid state could be of great interest for the assembly of coordination polymers on multiple N-coordinated triazole ligands at one metal ion. Therefore, the dimerization equilibrium in solution was investigated by ^{1}H NMR and UV/Vis spectrometry as well as cyclic voltammetry. Variable temperature ^{1}H NMR demonstrated that at concentrations of about 0.02 mol/L, the dimer at 4.79 ppm prevails (Figure 5, right), while the monomer is detected at 5.48 ppm. A dimerization constant K_D of 290 L/mol was determined at 25 °C and a Van't-Hoff plot of K_D at decreasing temperatures resulted a ΔH value of −10.63 kcal/mol and ΔS of −23.6 cal/mol·K (Figure S89). In contrast, in UV/Vis spectroscopy at about 2×10^{-4} mol/L in CH_2Cl_2 the monomer is dominant. The violet crystals yielded a dark blue solution. Two absorption bands, at 485 nm and 619 nm, respectively, were observed in the visible range. For the solid state, reflectance UV/Vis spectroscopy was carried out (Figure 5, left). The absorption bands at 351 nm and 510 nm apparently belong to the dimer $(\mathbf{10})_2$. Accordingly, the strongest absorption band at 619 nm is assigned to a dithiolate-π to Co^{III} charge transfer in the monomer **10**. Compared to the complex $[(\eta^5\text{-}C_5H_5)Co(bdt)]$ (λ = 566 nm), the band is bathochromicly shifted by 1500 cm^{-1}. [44] This difference can be attributed to the stronger dithiolate character in 1*H*-1,2,3-triazole-4,5-dithiolate ligands compared with the benzene-1,2-dithiolate, which shows a stronger conjugation to the aromatic system due to better electronegativity matching. Comparable charge transfer bands were reported for many other semi-sandwich complexes with a cobalt dithiolene ligand. [45–47] As expected, the equilibrium between the monomer and the dimer can be influenced by changing the temperature between 0 °C and 40 °C. An increased temperature results in an increased concentration of the monomer at 619 nm.

The cyclic voltammograms of **10** were measured at a concentration range, at which the dimer $(\mathbf{10})_2$ is the main species (Figure 6). The signal at a potential $E_{1/2}$ of −0.99 V for the Co^{III}/Co^{II} redox couple exhibits quasi-reversible features. The peak difference increases from 370 mV at a scan rate of 100 mV/s to 520 mV at 300 mV/s, which supports a weakly coupled two-electron process for $(\mathbf{10})_2$. In addition, irreversible oxidation at about +0.8 V causes the appearance of a new signal at slightly higher potential compared with the

original Co^{II}/Co^{III} couple. This can reasonably be assigned to the monomer, because, being easier to reduce, the 16 valence electron monomer **10** should exhibit a higher potential. Apparently, one-electron oxidation leads to a release of the monomer **10**.

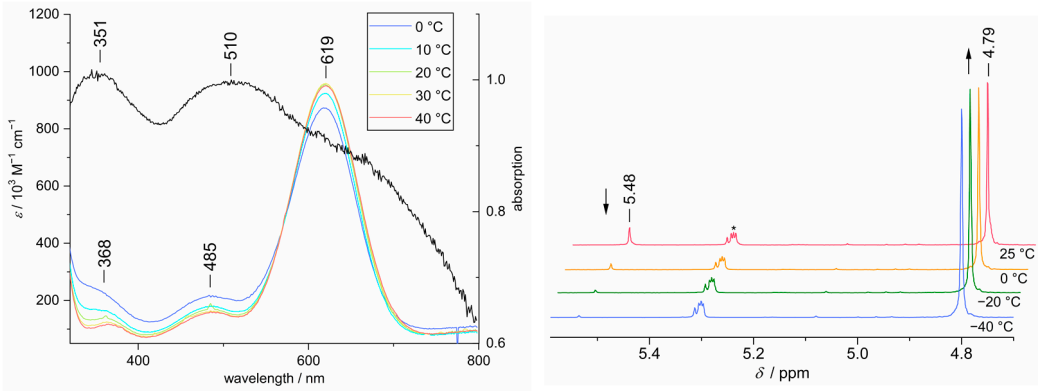

Figure 5. Temperature dependent spectra of **10**/(**10**)$_2$: UV/Vis spectra in CH_2Cl_2 solution and solid state (**left**) and ^{1}H NMR spectra in CD_2Cl_2 (*) (**right**).

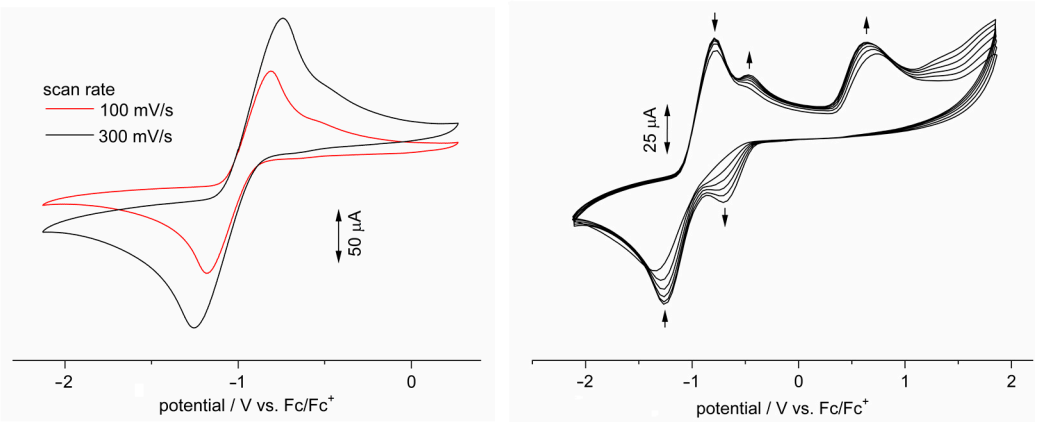

Figure 6. Cyclic voltammograms of the compound **10** in CH_2Cl_2 at different scan rates (**left**) and changes in the course of multiple potential scans (**right**).

4. Conclusions

In this publication, a new synthetic route for the assembly of 1*H*-1,2,3-triazole-4,5-dithiolenes was presented, which made use of click chemistry. Instead of complicated, expensive and sensitive catalysts, very high yields of the mono-substituted triazole sulfides **1** could be achieved using $CuSO_4$ in CuAAC. The second sulfur substituent could be introduced by facile deprotonation of the triazole ring and subsequent reaction with sulfur and benzyl bromide, yielding the triazole disulfides **2**. Nevertheless, this new synthetic method for the generation of a dithiolene unit at the 1*H*-1,2,3-triazole shows clear advantages in comparison with the synthesis described in the literature. [16] In addition, all attempts at a direct introduction of both sulfide substituents into the prototype 1*H*-1,2,3-triazole led exclusively to the monosulfide isomers **4**. Subsequent reductive removal of the S-protective groups with sodium in THF in the presence of naphthalene yielded the desired dithiol derivatives. However, by-products indicating a competing removal of the whole benzyl thiolate at either 4-or 5-position, respectively, were isolated in form of Co^{III} and Pt^{II} complexes (**11** and **12**). In coordination experiments with the dithiols, several complexes with Ni^{II}, Pd^{II}, Pt^{II} and Co^{III} could be isolated and fully characterized. It was shown that dithiolate coordination dominates the coordination behavior. Neither the coordinated metal (**6**, **7**, **8**) nor the protective group at the nitrogen atom of the triazole (**9a**–**c**) have a strong effect on the electronic situation at the dithiolate unit. With coordination of the [(η^5-C_5H_5)Co] moiety, a 16 valence electron Co^{III} center could be introduced at the

dithiolate unit giving complex **10**. Instead of a conceivable coordination of a triazole N atom, this complex showed a dimerization via dual μ-sulfur coordination in the solid state. By means of a temperature-dependent NMR and UV/Vis spectroscopic measurements completed by cyclic voltammetry, the thermodynamic parameters of the monomer–dimer equilibrium were determined.

Supplementary Materials: The following supporting information can be downloaded at: https://www.mdpi.com/article/10.3390/chemistry5020086/s1, Tables S1–S4: Crystallographic details for **1d, 1g, 2a, 6–9b** and **10–12**; Figure S1: Molecular structure of **1d** in the crystal; Figure S2: Molecular structure of **1g** in the crystal; Figure S3: Molecular structure of **2a** in the crystal; Figure S4: Molecular structure of **9a** in the crystal; Figure S5: Molecular structure of **9b** in the crystal; Materials, Measurements and Synthese of organic products (**1–4**); Figure S6: ^{1}H NMR spectrum (300 MHz) of 2,4-dimethoxybenzyl azide in $CDCl_3$ at 298 K; Figure S7: IR spectroscopy of 2,4-dimethoxybenzyl azide in THF; Figure S8: ^{1}H NMR spectrum (300 MHz) of 2-(trimethylsilyl)ethyl azide with traces of *n*-hexane in $CDCl_3$ at 298 K; Figure S9: ^{13}C NMR spectrum (75 MHz) of 2-(trimethylsilyl)ethyl azide with traces of n-hexane in $CDCl_3$ at 298 K; Figure S10: ^{29}Si NMR spectrum (60 MHz) of 2-(trimethylsilyl)ethyl azide in $CDCl_3$ at 298 K; Figure S11: IR spectroscopy of 2-(trimethylsilyl)ethyl azide in Et_2O with traces of DMF; Figure S12: ^{1}H NMR spectrum (500 MHz) of **1a** in $CDCl_3$ at 298 K; Figure S13: ^{13}C NMR spectrum (125 MHz) of **1a** in $CDCl_3$ at 298 K; Figure S14: IR spectroscopy of **1a** in CH_2Cl_2; Figure S15: ^{1}H NMR spectrum (300 MHz) of **1b** in acetone-D_6 at 298 K; Figure S16: ^{13}C NMR spectrum (75 MHz) of **1b** in $CDCl_3$ at 298 K; Figure S17: IR spectroscopy of **1b** in CH_2Cl_2; Figure S18: ^{1}H NMR spectrum (300 MHz) of **1c** in $CDCl_3$ at 298 K; Figure S19: ^{13}C NMR spectrum (75 MHz) of **1c** in $CDCl_3$ at 298 K; Figure S20: ^{29}Si NMR spectrum (60 MHz) of **1c** in $CDCl_3$ at 298 K; Figure S21: ^{1}H NMR spectrum (300 MHz) of **1d** in $CDCl_3$ at 298 K; Figure S22: ^{13}C NMR spectrum (75 MHz) of **1d** in $CDCl_3$ at 298 K; Figure S23: IR spectroscopy of **1d** in CH_2Cl_2; Figure S24: ^{1}H NMR spectrum (500 MHz) of **1e** in $CDCl_3$ at 298 K; Figure S25: ^{13}C NMR spectrum (75 MHz) of **1e** in $CDCl_3$ at 298 K; Figure S26: IR spectroscopy of **1e** in CH_2Cl_2; Figure S27: ^{1}H NMR spectrum (300 MHz) of **1f** in acetone-D_6 at 298 K; Figure S28: ^{13}C NMR spectrum (75 MHz) of **1f** in acetone-D_6 at 298 K: Figure S29: IR spectroscopy of **1f** in CH_2Cl_2; Figure S30: ^{1}H NMR spectrum (300 MHz) of **1g** in $CDCl_3$ at 298 K; Figure S31: ^{13}C NMR spectrum (75 MHz) of **1g** in $CDCl_3$ at 298 K; Figure S32: ^{1}H NMR spectrum (250 MHz) of **2a** with traces of EtOAc in $CDCl_3$ at 298 K; Figure S33: ^{13}C NMR spectrum (75 MHz) of **2a** in $CDCl_3$ at 298 K; Figure S34: IR spectroscopy of **2a** in CH_2Cl_2; Figure S35: ^{1}H NMR spectrum (300 MHz) of **2b** in $CDCl_3$ at 298 K; Figure S36: ^{13}C NMR spectrum (75 MHz) of **2b** in $CDCl_3$ at 298 K; Figure S37: IR spectroscopy of **2b** in CH_2Cl_2; Figure S38: ^{1}H NMR spectrum (300 MHz) of **2c** in $CDCl_3$ at 298 K; Figure S39: ^{13}C NMR spectrum (75 MHz) of **2c** in $CDCl_3$ at 298 K; Figure S40: ^{29}Si NMR spectrum (60 MHz) of **2c** in $CDCl_3$ at 298 K; Figure S41: IR spectroscopy of **2c** in CH_2Cl_2; Figure S42: ^{1}H NMR spectrum (300 MHz) of **2d** in $CDCl_3$ at 298 K; Figure S43: IR spectroscopy of **2d** in CH_2Cl_2; Figure S44: ^{1}H NMR spectrum (500 MHz) of **2e** in CD_2Cl_2 at 298 K; Figure S45: IR spectroscopy of **2e** in CH_2Cl_2; Figure S46: ^{1}H NMR spectrum (500 MHz) of **2f** in $CDCl_3$ at 298 K; Figure S47: ^{13}C NMR spectrum (126 MHz) of **2f** in $CDCl_3$ at 298 K; Figure S48: IR spectroscopy of **2f** in CH_2Cl_2; Figure S49: ^{1}H NMR spectrum (300 MHz) of **3** in $CDCl_3$ at 298 K; Figure S50: ^{13}C NMR spectrum (75 MHz) of **3** in $CDCl_3$ at 298 K; Figure S51: IR spectroscopy of **3** in CH_2Cl_2; Figure S52: ^{1}H NMR spectrum (300 MHz) of **4** in $CDCl_3$ at 298 K; Figure S53: ^{13}C NMR spectrum (75 MHz) of **4** in $CDCl_3$ at 298 K; Figure S54: IR spectroscopy of **4** in CH_2Cl_2; Figure S55: ^{1}H NMR spectrum (300 MHz) of **5a** in $CDCl_3$ at 298 K; Figure S56: IR spectroscopy of **5a** in CH_2Cl_2; Figure S57: ^{1}H NMR spectrum (300 MHz) of **5b** in CD_2Cl_2 at 298 K; Figure S58: IR spectroscopy of **5b** in CH_2Cl_2; Figure S59: ^{1}H NMR spectrum (300 MHz) of **5c** in THF-D_8 at 298 K; Figure S60: ^{1}H NMR spectrum (300 MHz) of **6** with traces of CH_2Cl_2 in $CDCl_3$ at 298 K; Figure S61: ^{13}C NMR spectrum (75 MHz) of **6** in $CDCl_3$ at 298 K; Figure S62: ^{31}P NMR spectrum (122 MHz) of **6** in $CDCl_3$ at 298 K; Figure S63: IR spectroscopy of **6** in CH_2Cl_2; Figure S64: ^{1}H NMR spectrum (300 MHz) of **7** with traces of CH_2Cl_2 and CH_3OH in DMF-D_7 at 298 K; Figure S65: ^{13}C NMR spectrum (75 MHz) of **7** in DMF-D_7 at 298 K; Figure S66: ^{1}H NMR spectrum (122 MHz) of **7** in DMF-D_7 at 298 K; Figure S67: IR spectroscopy of **7** in CH_2Cl_2; Figure S68: ^{1}H NMR spectrum (300 MHz) of **8** in CD_2Cl_2 at 298 K; Figure S69: ^{13}C NMR spectrum (75 MHz) of **8** in CD_2Cl_2 at 298 K; Figure S70: ^{31}P NMR spectrum (122 MHz) of **8** in CD_2Cl_2 at 298 K; Figure S71: IR spectroscopy of **8** in CH_2Cl_2; Figure S72: ^{1}H NMR spectrum (500 MHz) of **9a** with traces of CH_2Cl_2 in CD_2Cl_2 at 298 K; Figure S73: ^{13}C NMR spectrum (125 MHz) of **9a** in CD_2Cl_2 at 298 K; Figure S74: ^{31}P NMR spectrum (202 MHz) of **9a** in CD_2Cl_2 at 298 K; Figure S75: IR spectroscopy of **9a** in CH_2Cl_2; Figure S76: ^{1}H NMR spectrum (500 MHz) of **9b** with traces of CH_2Cl_2 in CD_2Cl_2 at 298 K; Figure S77**:** ^{13}C NMR spectrum

(125 MHz) of **9b** in CD_2Cl_2 at 298 K; Figure S78: ^{31}P NMR spectrum (202 MHz) of **9b** in CD_2Cl_2 at 298 K; Figure S79: IR spectroscopy of **9b** in CH_2Cl_2; Figure S80: ^{1}H NMR spectrum (500 MHz) of **9c** with traces of CH_2Cl_2 in CD_2Cl_2 at 298 K; Figure S81: ^{13}C NMR spectrum (125 MHz) of **9c** in CD_2Cl_2 at 298 K; Figure S82: ^{29}Si NMR spectrum (99 MHz) of **9c** in CD_2Cl_2 at 298 K; Figure S83: ^{31}P NMR spectrum (202 MHz) of **9c** in CD_2Cl_2 at 298 K; Figure S84: IR spectroscopy of **9c** in CH_2Cl_2; Figure S85: ^{1}H NMR spectrum (500 MHz) of **10** in $CDCl_3$ at 298 K; Figure S86: ^{13}C NMR spectrum (125 MHz) of **10** in $CDCl_3$ at 298 K; Figure S87: ^{29}Si NMR spectrum (99 MHz) of **10** in $CDCl_3$ at 298 K; Figure S88: IR spectroscopy of **10** in CH_2Cl_2; Figure S89: Van't-Hoff-plot of the monomer-dimer equilibrium **10**/(**10**)$_2$. References [25,48–63] are cited in Supplementary Materials.

Author Contributions: Investigation, visualization, writing and review & editing N.P. and W.W.S.; X-ray diffractometry and structure solution, A.V.; conceptualization and supervision W.W.S. All authors have read and agreed to the published version of the manuscript.

Funding: This research received no external funding.

Data Availability Statement: CCDC 225417-2254527 contain the supplementary crystallographic data for this paper. These data can be obtained free of charge via www.ccdc.cam.ac.uk/data_request/cif (accessed on 10 April 2023), or by emailing data_request@ccdc.cam.ac.uk, or by contacting The Cambridge Crystallographic Data Center, 12 Union Road, Cambridge CB2 1EZ, UK, fax: +44-1223-226033.

Conflicts of Interest: The authors declare no conflict of interest.

References

1. Peplow, M. Click and bioorthogonal chemistry win 2022 Nobel Prize in Chemistry. *Chem. Eng. News* **2022**, *36*, 3.
2. Kolb, H.C.; Finn, M.G.; Sharpless, K.B. Click Chemistry: Diverse Chemical Function from a Few Good Reactions. *Angew. Chem. Int. Ed.* **2001**, *40*, 2004–2021. [CrossRef]
3. Lewis, W.G.; Green, L.G.; Grynszpan, F.; Radić, Z.; Carlier, P.R.; Taylor, P.; Finn, M.G.; Sharpless, K.B. Click Chemistry In Situ: Acetylcholinesterase as a Reaction Vessel for the Selective Assembly of a Femtomolar Inhibitor from an Array of Building Blocks. *Angew. Chem. Int. Ed.* **2002**, *41*, 1053–1057. [CrossRef]
4. Ramachary, D.B.; Barbas, C.F. Towards Organo-Click Chemistry: Development of Organocatalytic Multicomponent Reactions Through Combinations of Aldol, Wittig, Knoevenagel, Michael, Diels-Alder and Huisgen Cycloaddition Reactions. *Chem. Eur. J.* **2004**, *10*, 5323–5331. [CrossRef]
5. Rostovtsev, V.V.; Green, L.G.; Fokin, V.V.; Sharpless, K.B. A Stepwise Huisgen Cycloaddition Process: Copper(I)-Catalyzed Regioselective "Ligation" of Azides and Terminal Alkynes. *Angew. Chem. Int. Ed.* **2002**, *41*, 2596–2599. [CrossRef]
6. Clarke, D.; Mares, R.W.; McNab, H. Preparation and pyrolisis of 1-(pyrazol-5-yl)-1,2,3-triazoles and related compounds. *J. Chem. Soc. Parkin Trans. 1* **1997**, 1799–1804. [CrossRef]
7. Huisgen, R. 1,3-Dipolar Cycloadditions. Past and Future. *Angew. Chem. Int. Ed. Engl.* **1963**, *2*, 565–598. [CrossRef]
8. Qin, A.; Jim, C.K.W.; Lu, W.; Lam, J.W.Y.; Häussler, M.; Dong, Y.; Sung, H.H.Y.; Williams, I.D.; Wong, G.K.L.; Tang, B.Z. Click Polymerization: Facile Synthesis of Functional Poly(aroyltriazole)s by Metal-Free, Regioselective 1,3-Dipolar Polycycloaddition. *Macromolecules* **2007**, *40*, 2308–2317. [CrossRef]
9. Jasiński, R. Nitroacetylene as dipolarophile in 2 + 3 cycloaddition reactions with allenyl-type three-atom components: DFT computational study. *Monatsh. Chem.* **2015**, *146*, 591–599. [CrossRef]
10. Hein, J.E.; Fokin, V.V. Copper-catalyzed azide-alkyne cycloaddition (CuAAC) and beyond: New reactivity of copper(I) acetylides. *Chem. Soc. Rev.* **2010**, *39*, 1302–1315. [CrossRef]
11. Beerhues, J.; Aberhan, H.; Streit, T.-N.; Sarkar, B. Probing Electronic Properties of Triazolylidenes through Mesoionic Selones, Triazolium Salts, and Ir-Carbonyl-Triazolylidene Complexes. *Organometallics* **2020**, *39*, 4557–4564. [CrossRef]
12. Tran, H.-V.; Haghdoost, M.M.; Poulet, S.; Tcherkawsky, P.; Castonguay, A. Exploiting *exo* and *endo* furan-maleimide Diels-Alder linkages for the functionalization of organoruthenium complexes. *Dalton Trans.* **2022**, *51*, 2214–2218. [CrossRef]
13. Crowley, J.D.; Bandeen, P.H.; Hanton, L.R. A one pot multi-component CuAAC "click" approach to bidentate and tridentate pyridyl-1,2,3-triazole ligands: Synthesis, X-ray structures and copper(II) and silver(I) complexes. *Polyhedron* **2010**, *29*, 70–83. [CrossRef]
14. Struthers, H.; Mindt, T.L.; Schibli, R. Metal chelating systems synthesized using the copper(I) catalyzed azide-alkyne cycloaddition. *Dalton Trans.* **2010**, *39*, 675–696. [CrossRef]
15. Haas, A.; Krächter, H.-U. Darstellung und Reaktionen Trifluormethylchalkogenyl-substituierter Alkine. *Chem. Ber.* **1988**, *121*, 1833–1840. [CrossRef]
16. Schallenberg, D.; Pardemann, N.; Villinger, A.; Seidel, W.W. Synthesis and coordination behaviour of 1*H*-1,2,3-triazole-4,5-dithiolates. *Dalton Trans.* **2022**, *51*, 13681–13691. [CrossRef]

17. Szilagyi, R.K.; Lim, B.S.; Glaser, T.; Holm, R.H.; Hedman, B.; Hodgson, K.O.; Solomon, E.I. Description of the Ground State Wave Functions of Ni Dithiolenes Using Sulfur K-edge X-ray Absorption Spectroscopy. *J. Am. Chem. Soc.* **2003**, *125*, 9158–9169. [CrossRef]
18. Lim, B.S.; Fomitchev, D.V.; Holm, R.H. Nickel Dithiolenes Revisited: Structures and Electron Distribution from Density Functional Theory for the Three-Member Electron-Transfer Series $[Ni(S_2C_2Me_2)_2]^{0,1-,2-}$. *Inorg. Chem.* **2001**, *40*, 4257–4262. [CrossRef]
19. Aragoni, M.C.; Caltagirone, C.; Lippolis, V.; Podda, E.; Slawin, A.M.Z.; Woollins, J.D.; Pintus, A.; Arca, M. Diradical Character of Neutral Heteroleptic Bis(1,2-dithiolene) Metal Complexes: Case Study of [Pd(Me_2timdt)(mnt)] (Me_2timdt = 1,3-Dimethyl-2,4,5-trithioxoimidazolidine; mnt^{2-} = 1,2-Dicyano-1,2-ethylenedithiolate). *Inorg. Chem.* **2020**, *59*, 17385–17401. [CrossRef]
20. Schallenberg, D. *Der Aufbau Polynuklearer Komplexe auf der Basis N-Heterozyklischer Dithiolene*; Universität Rostock: Rostock, Germany, 2013; pp. 1–49.
21. Ding, S.; Jia, G.; Sun, J. Iridium-Catalyzed Intermolecular Azide-Alkyne Cycloaddition of Internal Thioalkynes under Mild Conditions. *Angew. Chem. Int. Ed.* **2014**, *53*, 1877–1880. [CrossRef]
22. Haldón, E.; Nicasio, M.C.; Pérez, P.J. Copper-catalysed azide-alkyne cycloadditions (CuAAC): An update. *Org. Biomol. Chem.* **2015**, *13*, 9528–9550. [CrossRef] [PubMed]
23. Kappe, C.O.; Van der Eycken, E. Click chemistry under non-classical reaction conditions. *Chem. Soc. Rev.* **2010**, *39*, 1280–1290. [CrossRef] [PubMed]
24. Tornøe, C.W.; Christensen, C.; Meldal, M. Peptidotriazoles on Solid Phase: [1,2,3]-Triazoles by Regiospecific Copper(I)-Catalyzed 1,3-Dipolar Cycloadditions of Terminal Alkynes to Azides. *J. Org. Chem.* **2002**, *67*, 3057–3064. [CrossRef] [PubMed]
25. Seidel, W.W.; Meel, M.J.; Schaffrath, M.; Pape, T. In Pursuit of an Acetylenedithiolate Synthesis. *Eur. J. Org. Chem.* **2007**, *2007*, 3526–3532. [CrossRef]
26. Rasmussen, L.K.; Boren, B.C.; Fokin, V.V. Ruthenium-Catalyzed Cycloaddition of Aryl Azides and Alkynes. *Org. Lett.* **2007**, *9*, 5337–5339. [CrossRef]
27. Zhang, L.; Chen, X.; Xue, P.; Sun, H.H.Y.; Williams, I.D.; Sharpless, K.B.; Fokin, V.V.; Jia, G. Ruthenium-Catalyzed Cycloaddition of Alkynes and Organic Azides. *J. Am. Chem. Soc.* **2005**, *127*, 15998–15999. [CrossRef]
28. Boren, B.C.; Narayan, S.; Rasmussen, L.K.; Zhang, L.; Zhao, H.; Lin, Z.; Jia, G.; Fokin, V.V. Ruthenium-Catalyzed Azide-Alkyne Cycloaddition: Scope and Mechanism. *J. Am. Chem. Soc.* **2008**, *130*, 8923–8930. [CrossRef]
29. Landis, K.G.; Hunter, A.D.; Wagner, T.R.; Curtin, L.S.; Filler, F.L.; Jansen-Varnum, S.A. The synthesis and characterisation of Ni, Pd and Pt maleonitriledithiolate complexes: X-ray crystal structure of the isomorphous Ni, Pd and Pt ($Ph_2PCH_2CH_2PPh_2$)M(maleonitriledithiolate) congeners. *Inorg. Chim. Acta* **1998**, *282*, 155–162. [CrossRef]
30. Wrixon, J.D.; Hayward, J.J.; Raza, O.; Rawson, J.M. Oxidative addition chemistry of tetrathiocines: Synthesis, structures and properties of group 10 dithiolate complexes. *Dalton Trans.* **2014**, *43*, 2134–2139. [CrossRef]
31. Wrixon, J.D.; Ahmed, Z.S.; Anwar, M.U.; Beldjoudi, Y.; Hamidouche, N.; Hayward, J.J.; Rawson, J.M. Oxidative addition of *bis*-(dimethoxybenzo)-1,2,5,6-tetrathiocins to $Pt(PPh_3)_4$: Synthesis and structures of mono- and di-metallic platinum dithiolate complexes, (dmobdt)$Pt(PPh_3)_2$ and $[(dmobdt)Pt(PPh_3)]_2$. *Polyhedron* **2016**, *108*, 115–121. [CrossRef]
32. Miller, E.J.; Brill, T.B.; Rheingold, A.L.; Fultz, W.C. A Reversible Chemical Reaction in a Single Crystal. The Dimerization of (η^5-C_5H_5)Co($S_2C_6H_4$). *J. Am. Chem. Soc.* **1983**, *105*, 7580–7584. [CrossRef]
33. Nomura, M.; Sasao, T.; Hashimoto, T.; Sugiyama, T.; Kajitani, M. Structures and electrochemistry of monomeric and dimeric CpCo(dithiolene) complexes with substituted benzene-1,2-dithiolate ligand. *Inorg. Chim. Acta* **2010**, *363*, 3647–3653. [CrossRef]
34. Vicente, R.; Ribas, J.; Solans, X.; Font-Alaba, M.; Mari, A.; de Loth, P.; Cassoux, P. Electrochemical, EPR, and crystal structure studies on mixed-ligand 4,5-Dimercapto-1,2-dithia-2-thione phosphine complexes of nickel, palladium and platinum, M(dmit)(dppe) and Pt(dmit)$(PPh_3)_2$. *Inorg. Chim. Acta* **1987**, *132*, 229–236. [CrossRef]
35. Lee, S.-K.; Shin, K.-S.; Noh, D.-Y.; Jeannin, O.; Barrière, F.; Bergamini, J.-F.; Fourmigué, M. Redox Multifunctionality in a Series of Pt^{II} Dithiolene Complexes of a Tetrathiafulvalene-Based Diphosphine Ligand. *Chem. Asian J.* **2010**, *5*, 169–176. [CrossRef]
36. Keefer, C.E.; Purrington, S.T.; Bereman, R.D.; Knight, B.W.; Bedgood, D.R., Jr.; Boyle, P.D. The synthesis and characterization of platinum monodithiolene complexes containing 1,3-dithiole-2-oxo-4,5-dithiolate ($dmid^{2-}$) and 1,3-dithiole-2-thione-4,5-dithiolate ($dmit^{2-}$). *Inorg. Chim. Acta* **1998**, *282*, 200–208. [CrossRef]
37. Habe, S.; Yamada, T.; Nankawa, T.; Mizutani, J.; Murata, M.; Nishihara, H. Synthesis, Structure, and Dissociation Equilibrium of Co(η^5-C_5H_5)$(Se_2C_6H_4)_2$, a Novel Metalladiselenolene Complex. *Inorg. Chem.* **2003**, *42*, 1952–1955. [CrossRef]
38. Nomura, M.; Fourmigué, M. Isostructural diamagnetic cobalt(III) and paramegnetic nickel(III) dithiolene complexes with an extended benzdithiolate core [CpM^{III}(bdtodt)] (M = Co and Ni). *J. Organomet. Chem.* **2007**, *692*, 2491–2499. [CrossRef]
39. Nomura, M.; Kondo, S.; Yamashita, S.; Suzuki, E.; Toyota, Y.; Alea, G.V.; Janairo, G.C.; Fujita-Takayama, C.; Sugiyama, T.; Kajitani, M. Sulfur-rich CpCo(dithiolene) complexes: Isostructural or non-isostructural couples of CpCo(III) with CpNi(III) dithiolene complexes. *J. Organomet. Chem.* **2010**, *695*, 2366–2375. [CrossRef]
40. Watanabe, L.K.; Ahmed, Z.S.; Hayward, J.J.; Heyer, E.; Macdonald, C.; Rawson, J.M. Oxidative addition of 1,2,5,6-Tetrathiocins to Co(I): A Re-Examination of Crown Ether Functionalized Benzene Dithiolate Cobalt(III) Complexes. *Organometallics* **2022**, *41*, 226–234. [CrossRef]
41. Yang, L.; Powell, D.R.; Houser, R.P. Structural variation in copper(I) complexes with pyridylmethylamide ligands: Structural analysis with a new four-coordinate geometry index, τ_4. *Dalton Trans.* **2007**, 955–964. [CrossRef]

42. Keefer, C.E.; Bereman, R.D.; Purrington, S.T.; Knight, B.W.; Boyle, P.D. The ^{195}Pt NMR of L_2Pt(1,2-dithiolene) Complexes. *Inorg. Chem.* **1999**, *38*, 2294–2302. [CrossRef]
43. Kimura, T.; Nakahodo, T.; Fujihara, H. Preparation and reactivity of benzo-1,2-dichalcogenete derivatives and their bis(triphenylphosphine)platinum complexes. *Heteroat. Chem.* **2018**, *29*, e21472. [CrossRef]
44. Takeo, A.; Yoshihiro, W.; Akiko, M.; Toru, K.; Hirobumi, U.; Masatsugu, K.; Kunio, S.; Akira, S. Photochemical Reduction of (η^5-Cyclopentadienyl)(1,2-disubstituted 1,2-ethylenedichalcogenolato)cobalt(III) and (η^5-Cyclopentadienyl)(1,2-benzenedithiolato)cobalt(III) Complexes in the Presence of Triethanolamine. *Bull. Chem. Soc. Jpn.* **1992**, *65*, 1047–1051. [CrossRef]
45. Matsuo, Y.; Ogumi, K.; Maruyama, M.; Nakagawa, T. Divergent Synthesis and Tuning of the Electronic Structures of Cobalt–Dithiolene–Fullerene Complexes for Organic Solar Cells. *Organometallics* **2014**, *33*, 659–664. [CrossRef]
46. Murata, M.; Habe, S.; Araki, S.; Namiki, K.; Yamada, T.; Nakagawa, N.; Nankawa, T.; Nihei, M.; Mizutani, J.; Kurihara, M. Synthesis of Heterometal Cluster Complexes by the Reaction of Cobaltadichalcogenolato Complexes with Groups 6 and 8 Metal Carbonyls. *Inorg. Chem.* **2006**, *45*, 1108–1116. [CrossRef]
47. Tsukada, S.; Kondo, M.; Sato, H.; Gunji, T. Fine electronic state tuning of cobaltadithiolene complexes by substituent groups on the benzene ring. *Polyhedron* **2016**, *117*, 265–272. [CrossRef]
48. Sheldrick, G.M. *SHELXS-2013, Program for Solution of Crystal Structure*; Universität Göttingen: Göttingen, Germany, 2013.
49. Sheldrick, G.M. *SHELXL-2013. Program for Refinement of Crystal Structure*; Universität Göttingen: Göttingen, Germany, 2013.
50. Sheldrick, G.M. SHELXT–Integrated space-group and crystal-structure determination. *Acta Crystallogr. A Found. Adv.* **2015**, *71*, 3–8. [CrossRef]
51. Kitano, H.; Choi, J.-H.; Ueda, A.; Ito, H.; Hagihara, S.; Kan, T.; Kawagishi, H.; Itami, K. Discovery of Plant Growth Stimulants by C-H Arylation of 2-Azahypoxanthine. *Org. Lett.* **2018**, *20*, 5684–5687. [CrossRef]
52. Tran, T.K.; Bricaud, Q.; Ocafrain, M.; Blanchard, P.; Roncali, J.; Lenfant, S.; Godey, S.; Vuillaume, D.; Rondeau, D. Thiolate chemistry: A powerful and versatile synthetic tool for immobilization/functionalization of oligothiophenes on a gold surface. *Chem. Eur. J.* **2011**, *17*, 5628–5640. [CrossRef]
53. Matake, R.; Niwa, Y.; Matsubara, H. Phase-vanishing method with acetylene evolution and its utilization in several organic syntheses. *Org. Lett.* **2015**, *17*, 2354–2357. [CrossRef]
54. Spencer, L.P.; Altwer, R.; Wei, P.; Gelmini, L.; Gauld, J.; Stephan, D.W. Pyridine− and Imidazole−Phosphinimine Bidentate Ligand Complexes: Considerations for Ethylene Oligomerization Catalysts. *Organometallics* **2003**, *22*, 3841–3854. [CrossRef]
55. Zanato, C.; Cascio, M.G.; Lazzari, P.; Pertwee, R.; Testa, A.; Zanda, M. Tricyclic Fused Pyrazoles with a 'Click' 1,2,3-Triazole Substituent in Position 3 Are Nanomolar CB_1 Receptor Ligands. *Synthesis* **2015**, *47*, 817–826. [CrossRef]
56. Howell, S.J.; Spencer, N.; Philp, D. Recognition-mediated regiocontrol of a dipolar cycloaddition reaction. *Tetrahedron* **2001**, *57*, 4945–4954. [CrossRef]
57. Wang, T.; Wang, C.; Zhou, S.; Xu, J.; Jiang, W.; Tan, L.; Fu, J. Nanovalves-Based Bacteria-Triggered, Self-Defensive Antibacterial Coating: Using Combination Therapy, Dual Stimuli-Responsiveness, and Multiple Release Modes for Treatment of Implant-Associated Infections. *Chem. Mater.* **2017**, *29*, 8325–8337. [CrossRef]
58. Kumar, A.S.; Ghule, V.D.; Subrahmanyam, S.; Sahoo, A.K. Synthesis of thermally stable energetic 1,2,3-triazole derivatives. *Chem. Eur. J.* **2013**, *19*, 509–518. [CrossRef]
59. Standley, E.A.; Smith, S.J.; Müller, P.; Jamison, T.F. A Broadly Applicable Strategy for Entry into Homogeneous Nickel(0) Catalysts from Air-Stable Nickel(II) Complexes. *Organometallics* **2014**, *33*, 2012–2018. [CrossRef]
60. Lobana, T.S.; Bawa, G.; Hundal, G.; Butcher, R.J.; Castineiras, A. The Influence of Substituents at C 2 Carbon of Thiosemicarbazones on the Bonding Pattern of Bis(diphenylphopshano)alkanes in Palladium(II) Complexes. *Z. Anorg. Allg. Chem.* **2009**, *635*, 1447–1453. [CrossRef]
61. Li, X.; Zha, M.-Q.; Gao, S.-Y.; Low, P.-J.; Wu, Y.-Z.; Gan, N.; Cao, R. Synthesis, photoluminescence, catalysis and multilayer film assembly of an ethynylpyridine platinum compound. *CrystEngComm* **2011**, *13*, 920–926. [CrossRef]
62. Ramos-Lima, F.J.; Quiroga, A.G.; Pérez, J.M.; Font-Bardia, M. Synthesis and Characterization of New Transplatinum Complexes Containing Phosphane Groups—Cytotoxic Studies in Cisplatin-Resistant Cells. *Eur. J. Inorg. Chem.* **2003**, *2003*, 1591–1598. [CrossRef]
63. Shapley, J.R. *Inorganic Syntheses*; Wiley-Interscience: Hoboken, NJ, USA, 2004; Volume 34.